Employing MoO_2@NiO heterojunction as a highly selective and efficient electrochemical ethanol-to-acetaldehyde conversion catalyst

Junhao Wu [a], Xiao Zhang [a], Sijia Ren [a], Xinhui Lu [a], Jiaxin Yang [a], Kui Li *[a]

a School of Materials Science and Engineering, University of Jinan, Jinan 250022, Shandong, China. mse_lik@ujn.edu.cn

Experimental

1. Synthesis

The NiOOH precursors were synthesized through room-temperature electrodeposition, followed by the formation of MoO_2@NiO/CC catalyst electrodes via chemical vapor deposition under an argon atmosphere, as illustrated in Figure 1. The process commenced with the rigorous pretreatment of conductive carbon cloth. This involved sequential ultrasonic cleaning in acetone, isopropanol, and deionized water for 15 minutes each, followed by thorough drying under vacuum.

In the electrodeposition procedure, a solution containing 6 mmol of $Ni(NO_3)_2·6H_2O$ (Shanghai Macklin Biochemical Co., Ltd.) and 6 mmol of NH_4F (Shanghai Macklin Biochemical Co., Ltd.) dissolved in 50 mL of deionized water was prepared. This solution was used in a three-electrode system, where the carbon cloth served as the working electrode, a carbon plate as the counter electrode, and a saturated silver chloride electrode as the reference electrode. The deposition was conducted at a potential of -1.4 V for 180 seconds to achieve precise control over the nanoparticle loading on the carbon fiber surface. Following deposition, the precursor materials were rinsed with deionized water and anhydrous ethanol, then dried in a vacuum oven at 80°C for 6 hours.

The NiOOH precursor electrodes were then placed over a crucible containing molybdenum oxide powder, with the deposited NiOOH facing downward, in a porcelain boat. The system was evacuated three times to remove air from the furnace chamber, followed by gas-phase deposition at 750°C under an argon atmosphere for 1 hour. This process yielded the MoO_2@NiO/CC catalyst. Control samples, NiO/CC and MoO_2/CC, were prepared under identical conditions, substituting NiOOH and MoO_2, respectively.

2. Characterizations

The size and morphology of the synthesized materials were examined using a JEM-1200EX (JEOL) transmission electron microscope. High-resolution transmission electron microscopy (HRTEM) and high-angle annular dark field scanning transmission electron microscopy (HAADF-STEM) analyses were performed on a JEM-2100 (JEOL) system equipped with energy-dispersive X-ray spectroscopy (EDS). Powder X-ray diffraction (XRD) patterns were acquired using a Bruker AXS D8-Advanced X-ray diffractometer with Cu Kα radiation (λ = 1.5418 Å) over a 2θ range from 10° to 90°. X-ray photoelectron spectroscopy (XPS) was conducted using an ESCALAB 250 (Thermo-Fisher Scientific) spectrometer.

3. Electrochemical Measurements for the EOR

Electrochemical measurements were conducted with a CHI 760E electrochemical workstation (Shanghai Chenhua Co., Ltd.) using a three-electrode setup at room temperature. The catalyst sample served as the working electrode, a platinum electrode was used as the counter electrode, and a mercury oxide electrode functioned as the reference electrode. Prior to testing, the electrolyte was purged with high-purity nitrogen for at least 30 minutes to remove any potential interfering gases. All potentials were converted to the reversible hydrogen electrode (RHE) scale based on the equation:

$$E\ (\text{vs. RHE}) = E\ (\text{vs. Ag/AgCl}) + 0.0591 \times \text{pH} + 0.1989$$

The scan rate of linear sweep voltammograms (LSV) and cyclic voltammetry (CV) are 5 mV/s and 10 mV/s, respectively. For the quantification of products from ethanol oxidation, 80 mL electrolyte was used each time. The samples catalyzed ethanol oxidation reaction at different potentials by chronoamperometry with controlling the same quantity of electric charge at same potential between different samples.

The working electrode was activated by cycling between -1.0 and 0.5 V (vs. Hg/HgO) at a scan rate of 100 mV/s in 1.0 M KOH for several cycles. Electrochemical surface areas (ECSAs) were determined through cyclic voltammetry (CV) measurements. The performance of the ethanol oxidation reaction (EOR)

was evaluated in a 1.0 M KOH + 1.0 M ethanol solution, with testing conducted between -0.9 and 0.3 V (vs. SCE) at a scan rate of 100 $mV \cdot s^{-1}$.

4. Determination of product yields and faradaic efficiencies

The concentration of produced acetaldehyde and acetic acid were detected and quantified by gas chromatograph (Agilent GC system-7890B with Headspace sampler-7697A) and ion chromatograph (Shenghan CIC-D100), respectively.The yield rates, Faradaic efficiencies (FE) and sensitivities of acetaldehyde and acetic acid were calculated by the following equation:

C_2H_4O yield = (c C_2H_4O × V) / $area_{cat}$.

$C_2H_4O_2$ yield = (c $C_2H_4O_2$ × V) / $area_{cat}$.

FE C_2H_4O = (2 × F × c C_2H_4O × V) / (44 × Q)

FE $C_2H_4O_2$ = (4 × F × c $C_2H_4O_2$ × V) / (60 × Q)

Selectivity C_2H_4O = n C_2H_4O / (n C_2H_4O + n $C_2H_4O_2$)

Selectivity $C_2H_4O_2$ = n $C_2H_4O_2$ / (n C_2H_4O + n $C_2H_4O_2$)

where c is the mass concentration of C_2H_4O and $C_2H_4O_2$; V is the volume of the electrolyte; areacat. is the geometric area of the samples; F is the Faraday constant and Q is the quantity of electric charge through the working electrode; n is the mole of C_2H_4O and $C_2H_4O_2$.

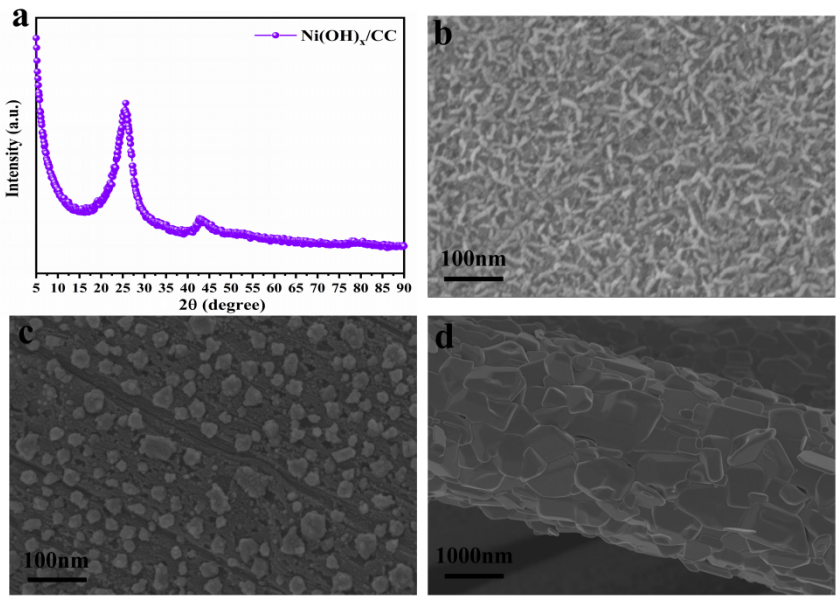

Figure. S1. (a) XRD pattern of the NiOOH/CC, SEM images of (b) NiOOH/CC and (c) NiO/CC and (d) MoO_2/CC.

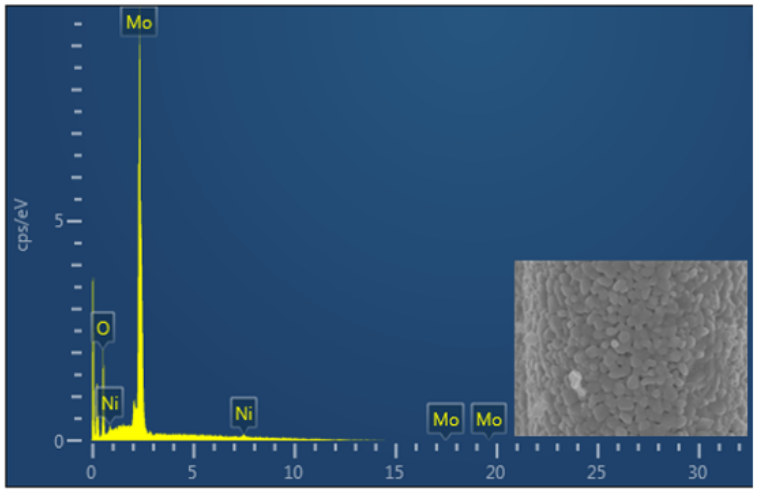

Element	wt%	At%
O	23.34	64.24
Ni	1.97	1.47
Mo	74.69	34.28

Figure S2. Chemical composition of MoO_2@NiO/CC by EDS

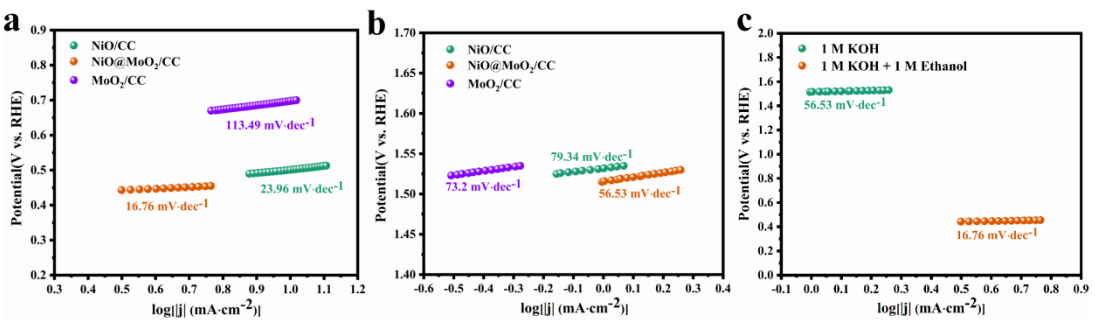

Figure. S3. Tafel plots of (a) NiO/CC, MoO_2@NiO/CC and MoO_2/CC in 1 M KOH with 1 M ethanol. (b) NiO/CC, MoO_2@NiO/CC and MoO_2/CC in 1 M KOH. (c) Comparisons of MoO_2@NiO/CC in 1 M KOH with and without 1 M ethanol.

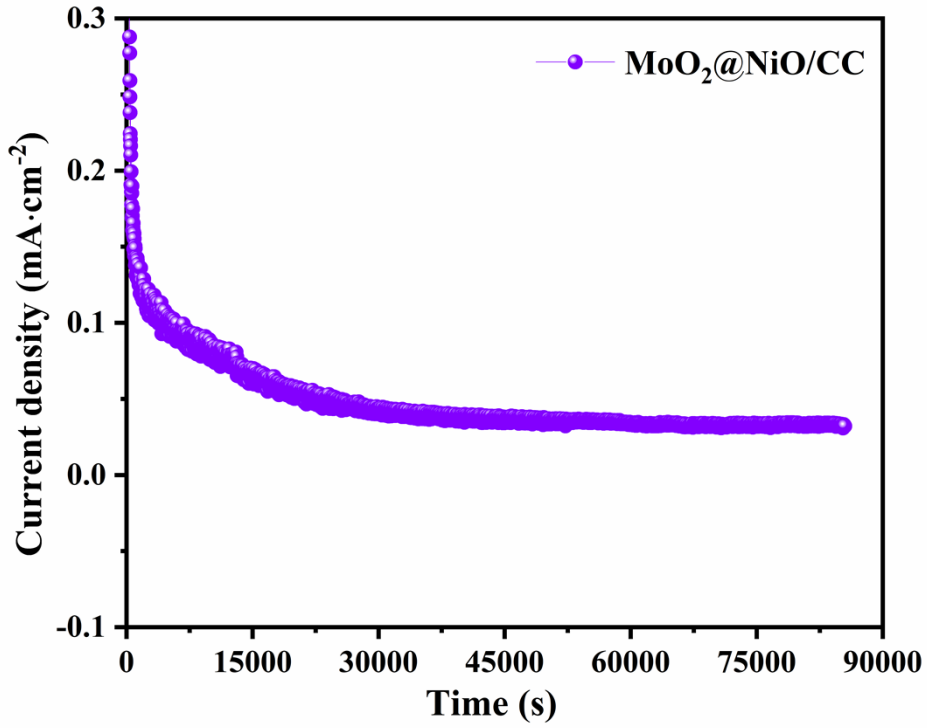

Figture S4. Chronoamperometric measurements of MoO_2@NiO/CC with 24 h in an alkaline electrolyte containing 1M ethanol

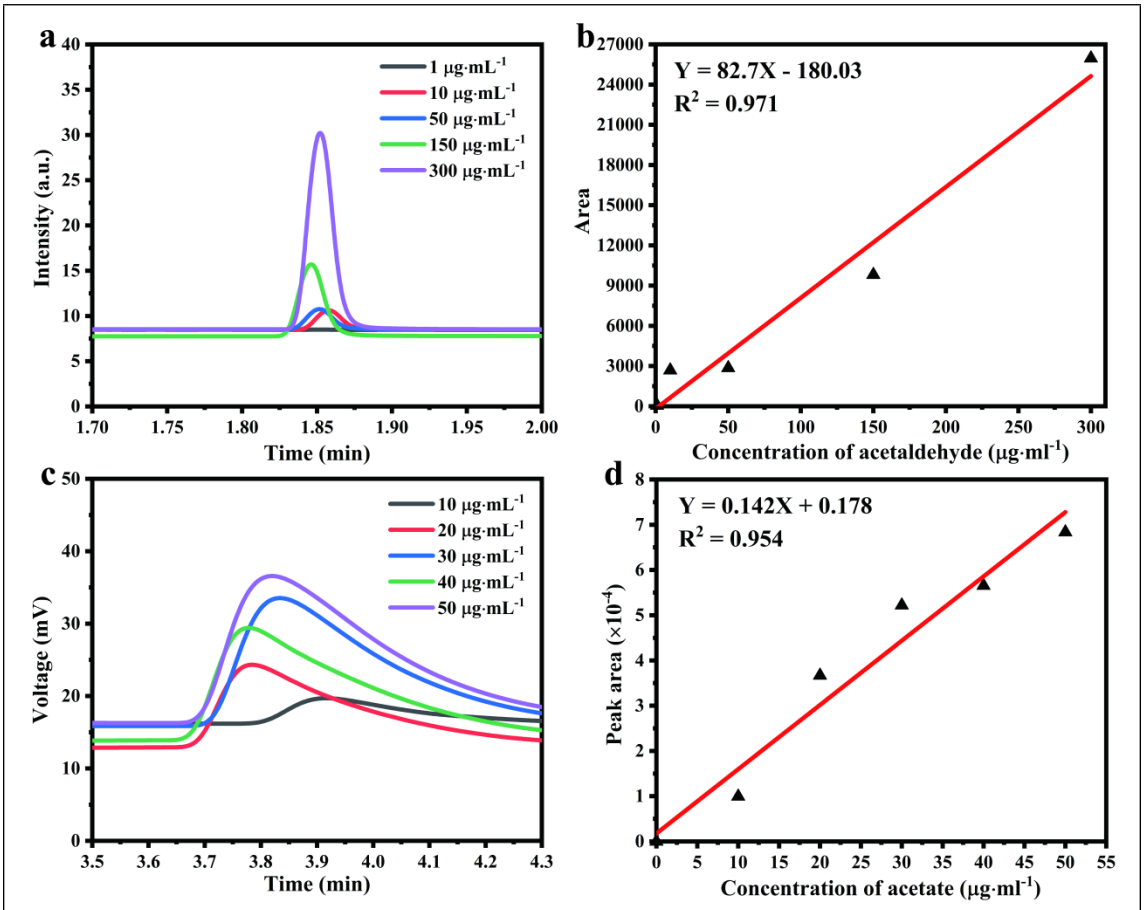

Figure S5 (a) GC curves of acetaldehyde standard solutions with different concentrations; (b) concentration-peak area standard curves of acetaldehyde; (c) IC curves of acetate standard solutions with different concentrations and (d) concentration-peak area standard curve of acetate.

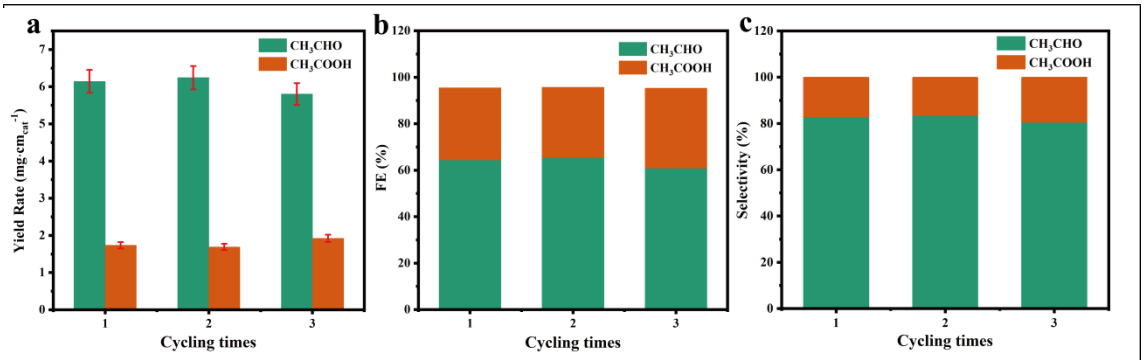

Figure S6. The yield rate, Faradaic efficiency and selectivity of cycling test for stability of MoO_2@NiO/CC. Each cycle consumes 120 C electricity at 1.41V.

Table S1. C, O, Ni and Mo contents in NiO/CC, MoO_2@NiO/CC and MoO_2/CC calculated from the overall survey scans of XPS measurement.

Atomic %	**NiO/CC**	**NiO@MoO_2/CC**	**MoO_2/CC**
C_{1s}	70.97	20.17	44.21
O_{1s}	18.41	38.94	29.38
Mo_{3d}	/	14.86	12.55
Ni_{2p}	4.85	1.47	/

Table S2. Peak position and peak area of XPS spectra of O 1s.

Catalyst		Lattice oxygen	Oxygen vacancy	Adsorbed water
NiO/CC	**Bindingenergy**	528.94eV	530.42 eV	532.19 eV
	Peakarea	5891.25	8335.84	15461.08
NiO@MoO_2/CC	**Bindingenergy**	539.66eV	530.39 eV	531.80 eV
	Peakarea	27879.49	24636.36	6891.87
MoO_2/CC	**Bindingenergy**	529.24 eV	530.29 eV	/
	Peakarea	27770.97	19593.05	/

Table S3. Peak position and peak area of XPS spectra of Ni 2p.

Catalyst		**Ni^0**		**Ni^{3+}**		**Ni^{2+}**	
NiO/CC	**Binding energy**	853.33 eV	870.88 eV	858.02eV	/	855.14 eV	872.77 eV
	Peakarea	8391.76	4378.94	2998.18	/	12404.65	7975.31
NiO@MoO_2/CC	**Binding energy**	/	/	857.49eV	875.75 eV	855.37 eV	873.06 eV
	Peakarea	/	/	3979.25	1244.70	7961.19	2823.34

Table S4. Peak position and peak area of XPS spectra of Mo 3d.

Catalyst		$3d_{5/2}$				$3d_{3/2}$		
		Mo^0	Mo^{2+}	Mo^{4+}	Mo^{5+}	Mo^{5+}		Mo^{6+}
MoO_2/CC	Binding energy	228.48 eV	231.72 eV	228.87 eV	230.40 eV	232.28 eV	233.42 eV	234.88 eV
	Peakarea	11135.41	10605.00	7541.16	18222.50	9291.52	16007.29	7590.28
Catalyst		Mo^{2+}	Mo^{4+}	Mo^{5+}		Mo^{5+}		Mo^{6+}
NiO@MoO_2/CC	Binding energy	/	228.97 eV	230.75 eV	232.24 eV	233.89 eV	/	235.36 eV
	Peakarea	/	13126.18	15155.84	28162.67	14304.70	/	14695.26

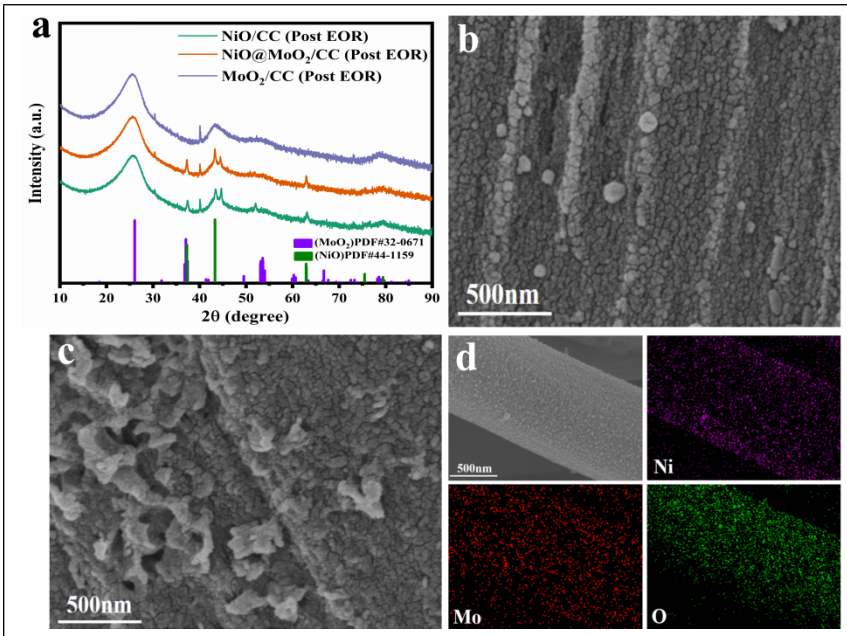

Figure. S7. (a) XRD pattern of the NiO/CC, MoO_2@NiO/CC and MoO_2/CC at post EOR, SEM images of (b) MoO_2/CC and (c) MoO_2@NiO/CC at post EOR; (d) EDS elemental mapping analysis of MoO_2@NiO/CC nanosheet at post EOR.

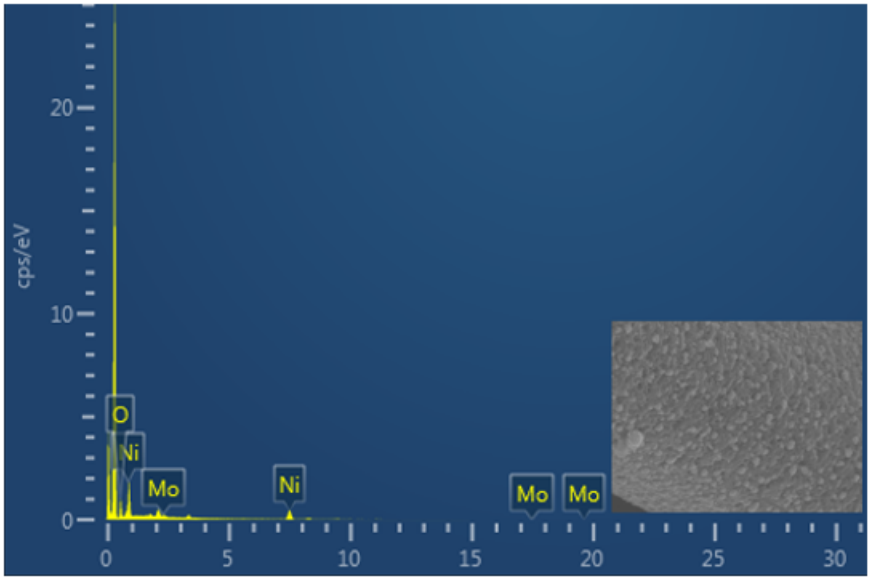

Element	wt%	At%
O	21.65	51.05
Ni	72.76	46.75
Mo	5.59	2.20

Figure S8. Chemical composition of MoO_2@NiO/CC by EDS at post EOR.

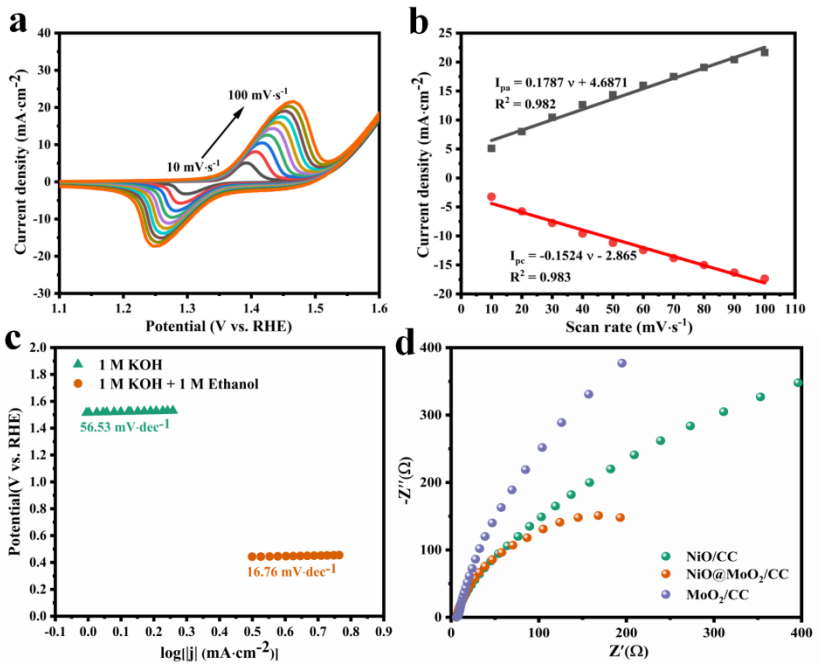

Figure S9. CV curves of (a) MoO_2@NiO/CC in 1 M KOH at increasing potential scan rates (10, 20, 30, 40, 50, 60, 70, 80, 90, and 100 mV·s^{-1}). Linear relationship between anodic (I_{pa}, black curve) and cathodic current (I_{pc}, red curve) densities and the scan rates of (b) MoO_2@NiO/CC. (c) Comparisons of MoO_2@NiO/CC in 1 M KOH with and without 1 M ethanol. (d) Electrochemical impedance spectroscopy plots of NiO/CC, MoO_2@NiO/CC and MoO_2/CC. Inset: the equivalent circuit. R_s: series resistance; R_{ct}: charge-transfer resistance; CPE: constant-phase element related to the double-layer capacitance.

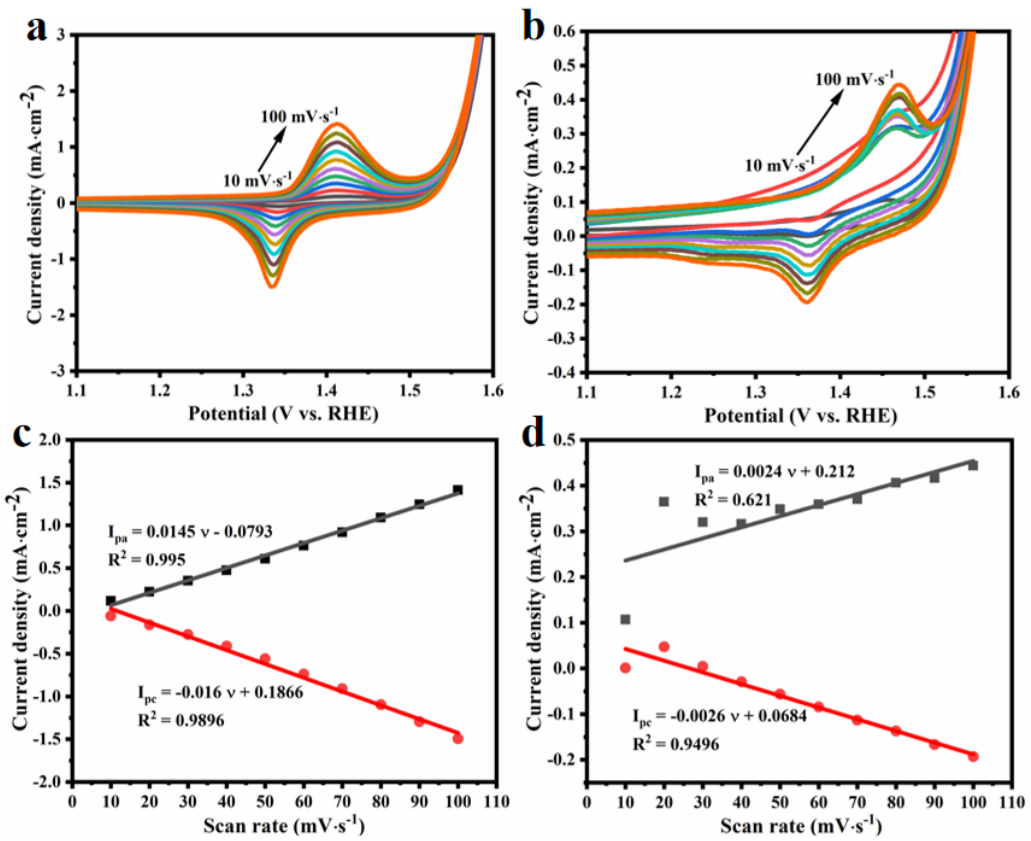

Figure S10. CV curves of (a) NiO/CC and (b) MoO_2/CC in 1 M KOH at increasing potential scan rates (10, 20, 30, 40, 50, 60, 70, 80, 90, and 100 mV·s-1). Linear relationship between anodic (Ipa, black curve) and cathodic current (Ipc, red curve) densities and the scan rates of (c) NiO/CC and (d) MoO_2/CC.

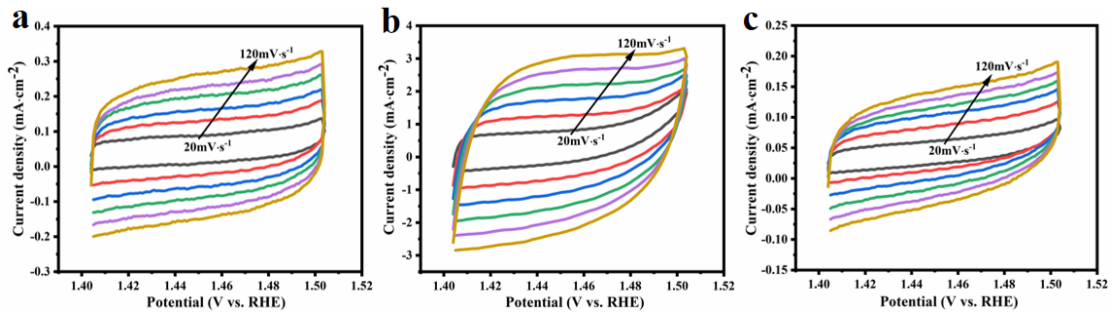

Figure S11. CV curves of (a) NiO/CC, (b) MoO_2@NiO/CC and (c) MoO_2/CC in 1 M KOH at different potential scan rates of 10, 20, 30, 40, 50, 60, 70, 80, 90, and 100 $mV \cdot s^{-1}$.

The ECSAs of the samples were estimated via the double layer capacitances (C_{dl}). First, CV scans were run at different scan rates in the non-faradic potential range of 1.4 V-1.5 V. Next, we plotted the collected Δj/2 against scan rate for each sample, and the Cdl can be obtained from the slopes. In this step, Δj was defined as:

$\Delta j = j_{anodic,\ 1.45\ V} - j_{cathodic,\ 1.45V}$

The ECSAs were then calculated based on the following equation:

$ECSA = (C_{dl} \cdot A_{geometric})/C_s$

where Ageometric is the geometric surface area of the glassy carbon electrode and C_s is the specific capacitance of a standard flat surface (40 μF·cm^{-2}).

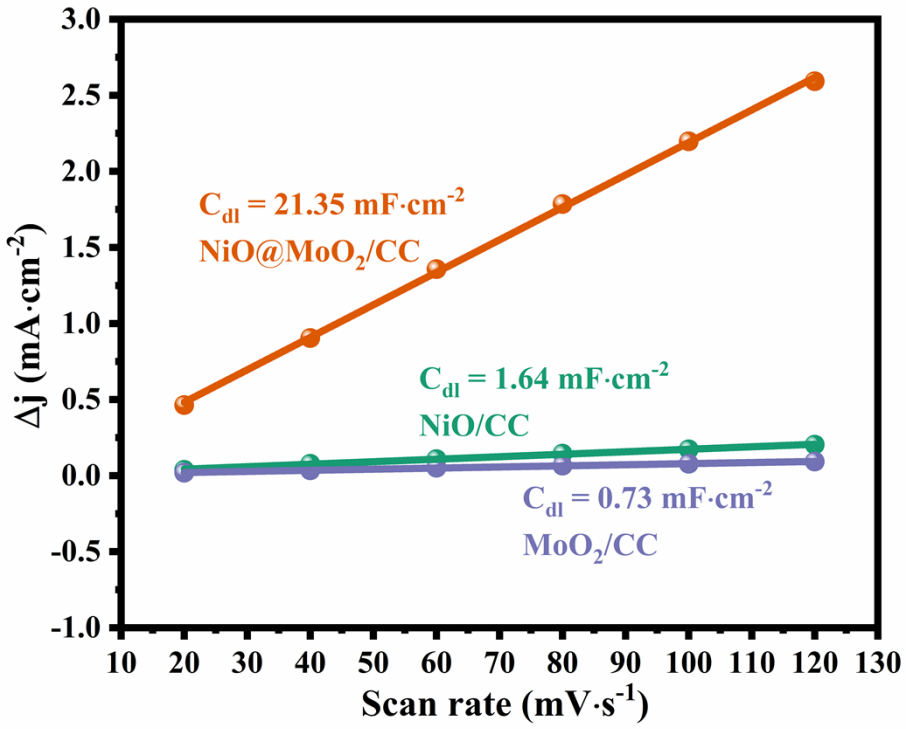

Figure S12. Calculations of double layer capacitances for NiO/CC, MoO_2@NiO/CC and MoO_2/CC.

Table S5. Cdl and ECSA values of NiO/CC, MoO_2@NiO/CC and MoO_2/CC.

Sample	**Cdl (mF cm^{-2})**	**ECSA (cm^2)**
NiO/CC	1.64	41
MoO_2@NiO/CC	21.35	533.74
MoO_2/CC	0.73	18.25

Table S6. Summary of electrocatalytic systems and their performance on selective oxidation of alcohols.

Electrocatalyst	***J*(mA cm^{-2})/*E*(V_{RHE})**	**Substrate/concentration**	**Product**	**Sel.**	**Faradic efficiency (FE)**	**Ref.**
MoO_2@NiO/CC	10/1.39	Ethanol/1 M	acetaldehyde	79.63%	60.02%	This work
Co_3O_4-air	10/1.46	Ethanol/1 M	acetaldehyde	79.63%	60.02%	8
Cu-doped NiOOH	227/1.72V	alcohols/1 M	acetate	-	98%	9
Co_3O_4 nanosheets	10/1.5 V	Ethanol/1.0 M	ethyl acetate	95%	-	10
CoNi hydroxide nanosheets	10mA/1.39 V	Ethanol/1 M	acetate	-	94.1%	11
Nickel chalcogenides	70.2/1.5	Ethanol/1 M	acetic acid	> 90%	-	12
Pd NPs@Ni SAC	70.2/1.5	Ethanol/1M	C1 pathway	28%	-	13
Pt/WO3 Nanosheets	-	Ethanol/0.5 M	CO_2	21.9%	-	14
PdxNby/C	-	Ethanol/1 M	CO_2	-	-	15
Pd/CuO–$Ni(OH)_2$/C	-	Ethanol/1 M	CO_2	22.5%	-	16
PtPb@PtIr 1HNPs	-	Ethanol/1 M	C1 pathway	-	57.93%	17
single-atom W-doped Pd metallene aerogels	-	Ethanol/1 M	C1 reaction pathway	-	25.8%	18
Fluorine-Modified FeOOH	10/1.43	Ethanol/1 M	acetic acid / unsaturated fatty acid and ethyl acetate	Main / Byproducts	-	19
PtPdRh/CNTs	1.04/0.6	Ethanol/1 M	C1 and C2 pathways	high	-	20
Au/Pd nanoparticles	10/1.52	Ethanol/1 M	C1 and C2 pathways	high	-	21
Pd/$CoNiO_2$/rGO	13.49/1.43	Ethanol/1 M	acetic acid	60.26%	-	22

References

1. Kresse G., Furthmüller, J. Efficiency of Ab-Initio Total Energy Calculations for Metals and Semiconductors Using a Plane-Wave Basis Set. Computational Materials Science, 1996, 6, 15−50.

2. Kresse G., Furthmüller J. Efficient Iterative Schemes for Ab Initio Total-Energy Calculations Using a Plane-Wave Basis Set. Physical Review B, 1996, 54, 11169−11186.

3. J Perdew，K Burke，M Ernzerhof. Generalized Gradient Approximation Made Simple. Physical Review Letters, 1996, 77, 3865−3868.

4. Kresse G., Joubert D. From Ultrasoft Pseudopotentials to the Projector Augmented-Wave Method. Physical Review B, 1999, 59, 1758-1775.

5. Blöchl P. E. Projector Augmented-Wave Method. Physical Review B, 1994, 50, 17953-17979.

6. S Grimme, J Antony, S Ehrlich, H Krieg, A consistent and accurate ab initio parametrization of density functional dispersion correction (DFT-D) for the 94 elements H-Pu. Journal of Chemical Physics, 2010, 132, 154104.

7. S Grimme, S Ehrlich, L Goerigk. Effect of the damping function in dispersion corrected density functional theory. Journal of Computational Chemistry, 2011，32, 1456-1465.

8. S L Dudarev, G A Botton, S Y Savrasov, C J Humphreys, A P Sutton. Electron – energy – loss spectra and the structural stability of nickel oxide: An LSDA + U study. Physical Review B, 1998，57, 1505–1509.

9. H Wang, A Guan, J Zhang, Y Mi, S Li, T Yuan, C Jing, L Zhang, L Zhang, G Zheng. Copper-doped nickel oxyhydroxide for efficient electrocatalytic ethanol oxidation. Chinese Journal of Catalysis, 2022,43(6),1478-1484.

10. L Dai, Q Qin, X Zhao, C Xu, C Hu, S Mo, Y O Wang, S Lin, Z Tang, N Zheng. Electrochemical partial reforming of ethanol into ethyl acetate using ultrathin Co_3O_4 nanosheets as a highly selective anode catalyst. ACS Central Science, 2016, 2(8): 538-544.

11. W Wang, Y B Zhu, Q Wen, Y Wang, J Xia, C Li, M W Chen, Y Liu, H Li, H A Wu, T Zhai. Modulation of molecular spatial distribution and chemisorption with perforated nanosheets for ethanol electro-oxidation. Advanced Materials, 2019, 31(28): 1900528.

12. Y Zhang, L Zhang, C Song, Y Qin, L Lu, W Zhu, Z Zhuang. Nickel chalcogenides as selective ethanol oxidation electro-catalysts and their structure–performance relationships. Chemical Communications, 2022, 58, 2496.

13. S Li, A Guan, H Wang, Y Yan, H Huang, C Jing, L Zhang, L Zhang, G Zheng. Hybrid palladium nanoparticles and nickel single atom catalysts for efficient electrocatalytic ethanol oxidation. Journal of Material Chemistry A, 2022, 10, 6129.